EVALUATION OF FALSE WALL FRUIT OIL AS A MEDIUM FOR THE AUSTEMPERING PROCESS OF DUCTILE CAST IRON

Ogbodo J.N*[1], Ameh E.M[1]. Agbo A.O[1], Ocheri C[2]
[1]Department of Metallurgical and Materials Engineering
Enugu State University of Science and Technology(ESUT),
Enugu State
Lead Author : Ogbodo J. N.
E - mail: joyogbodo429@yahoo.com
Phone no:08030476422

ABSTRACT

Evaluation of the false wall (Canarium Schweinfurthii) fruit oil as a quenching medium in the austempering process of ductile cast iron was investigated. As an alternative austempering medium, the false wall oil fruit was compared with the standard salt bath, as both were investigated for heat capacity and flame or adiabatic temperature (the maximum heat generated during the combustion process).

Unalloyed and alloyed ductile cast iron specimens were cut and machined from the 25mm Y-blocks cast for the study. The study confirmed that micro-alloyed ductile cast iron samples with additions of small percentages of (0.1, 0.2, 0.3 wt% molybdenum, 0.05, 0.10, 0.15wt% vanadium, and 0.15wt% a combination of both alloying elements) respectively, significantly improved the mechanical properties which was attributed to the heat treatment techniques of the oil quenching and isothermal tempering application that produced an ADI material with sound mechanical properties and micro-structural analysis.

The processing parameters used were: austenitizing temperature at 920 deg. C, holding time for 1hr, austempering temperature at 260 deg. C (lower bainite) at various austempering times of 1 - 4hrs in both oil and salt baths media for comparisons.

Mechanical property tests (tensile strength, elongation, hardness, and impact energy) of the austempered ductile cast iron were greatly improved upon. The optimum properties developed were obtained between 2.5hrs - 3hrs, which was the processing window for the material. The false wall fruit oil, which was investigated, showed an excellent property and reacted at the processing window which was narrower than the standard salt bath. The mechanical properties were at their best optimum at 3 hours austempering time of vanadium and molybdenum in the oil bath, as there was improved ductility and toughness and a slight reduction in hardness and tensile strength.

The micro-structure consisted of graphite nodules, which were surrounded by a circular ferrite and high carbon enrichment content in austenite called "ausferrite".

The false wall fruit oil could be used as an alternative replacement austempering medium to achieve the desired properties.

Keywords: Austenitized, soaked, austempering, matrix false wall fruit oil, austerity

1.0 Introduction

Heat treatment originated as an ancient art in man's attempt to improve the performance of materials in practical applications (Ause, 2008). Khanna (2002), pointed out that in the middle of the 19th century that more attentions were directed to develop the art and science of working, treating, and producing metals from its raw materials state to the final stage product(s) to suit various areas of application in order improve man's comfort. The final properties of alloys are not only due to their chemical compositions, but also due to their metallurgical history. It is possible to use different alloy treatments in order to change the properties, thus finding the easiest way of heat treatment(s) and optimum treatment conditions, which is of fundamental importance in achieving the desired properties (Fracasso,

2010). Metals and alloys develop requisite (necessary for a particular purpose) properties through heat treatments which plays a critical role in achieving the appropriate microstructures which imparts the desired characteristics in a given material (Shehu, 2016). The presence of these phases and their micro-structures, are of importance in deciding the resultant properties in the metal/alloy (Ause, 2008). Recently and over the years, the industrial use of ductile cast iron has increased and principally the use of austempered ductile cast iron (ADI). The ADI has enhanced mechanical properties which are extensively used in the fabrication of mechanical parts such as gears and crankshafts (Isah 2011). The ADI has become an established alternative in many industrial applications that were previously the exclusive domain of the steel family. Replacing the normal steel parts with ADIs results in several advantages which strongly promoted the acceptance and use of these materials, for example in the automotive industry. The first economic reason for the use of the ADIs, is that the original base material (nodular cast iron (the parent material to which a coating or electroplating, welding, and soldering is applied) is cheaper than steel. Secondly, the ADIs are castable materials; thus products can be moulded and re moulded thereby allowing cost reduction of the manufacturing process when compared to conventional steel machining (Martins, 2006). Austempered ductile cast iron (ADI) offers the design engineer the best combinations of low cost, design flexibility, good machinability, high strength-to-weight ratio and good toughness, wear resistance and fatigue strength (materials not yielding to failure due to fluctuating stresses/loads) (Tun & Lwin 2009). The capabilities of such newly formed materials are far superior to many ferrous and aluminium alloys. This "ausferrite," which is not created by traditional heat treatment techniques, shows twice, if not triple, the strength for a given degree of ductility when compared to ferritic, pearlitic, or even martensitic structures (Behara & Sohala, 2012). When austempered ductile cast irons were used in place of traditional steel parts, there were a number of benefits that greatly aided in the adoption and application of these materials, such as in the automotive industry (Isah, 2011). Gears that are made from ADI with close tolerances have been successfully used in engines and transmissions. Considerable efforts have been devoted to the development of automobile gears in Nigeria during the past years, to produce transmissions for engines made in Nigeria. Currently, many investigations are being carried out to characterise and improve the mechanical properties of ADI using the following hot liquid baths: nitrate/nitrite salts, lead, oils, and polymers. Among the liquid baths listed, austempering is the most typically carried out in a nitrate/nitrite salt bath due to the advantages it offers compared to others. Although a lot of attention is being given to vegetable oils, mineral oils, and polymer solutions. Oil quenching is a logical choice for gears.

2.0 Materials and Methods

This research work was conducted by considering all the metallurgical factors from materials selection to finishing and testing. Materials used for this research work were obtained from the: Scientific Equipment Development Institute (SEDI) Enugu, Enugu State Nigeria, Ahmadu Bello University Zaria (ABU), Kaduna State Nigeria, Nigeria Metallurgical Development Council (NMDC) Jos Plateau State, Nigeria Machine Tools Oshogbo Osun State, National Research Institute for Chemical Technology (NARICT) Zaria, Kaduna State, National Automotive Design and Development Council (NADDC) Zaria, The physical and chemical properties of the oil at No. 17 Udoka Housing Estate in Awka, Anambra State, from Vom Jos Souths Local Government Area Plateau State, Kaduna State. As an alternative to steel, they were utilised to assess the efficacy of False Wall (Canarium Schweinfurthii) fruit oil as a quenching medium in the austempering process of ductile cast iron.

2.1 Materials

Pure steel scrap (CRCA), ferro alloys (silicon, magnesium, vanadium and molybdenum), metallographic consumables (silicon carbide powder, alumina, cerium oxide, and etchants), graphite coke, silica sand (82%), mould boxes, bentonite (9%), pulverized clay (a special binder for good surface finishing; 5%), water (4%), and wooden pattern (Y-Blocks), were used for this study. The Optical emission spectrometer (GEMCO) was used to determine the chemical compostions of materials as indicated in Table 1 - 6

Table 1 Chemical compositions of the steel scrap (CRCA), wt%

C	Mn	S	P	Fe
0.05	0.3	0.03	0.03	Balance

Table 2: Chemical compositions of the graphite coke (Carbon), wt%

C	ASH	S	VOLATILE MATTER	MOISTURE
72	27.5	0.2	<0.5	0.1

Table 3 Chemical compositions of the magnesium-ferrosilicon (mg-fe-si) alloy, wt%

Mg	Si	Ca	RE	Al	Fe
10	44.76	2.02	0.8	<0.7	Balance

Table 4: Chemical compositions of the ferro-silicon (Fe-Si) alloy, wt%

Si	Al	C	S	P	Fe
75	0.31	0.0032	0.001	0.001	Bal

Table 5: Chemical compositions of the ferro-vanadium Alloy, Wt%

Vn	Fe	Si	Al	S
45.847	2.631	0.328	0.102	0.476

Table 6: Chemical compositions of ferro-molybdenum alloy, wt%

Mo	Fe	Si	Cu	S
61.82	2.797	0.259	0.686	0.0863

2.2 Methods/Procedures/Production of Ductile Cast Iron

2.2.1 Pattern

Wooden removable patterns were used to replicate the casting cavity according to ASTM A536 - 84 standards for test coupons. The pattern dimension took into account the 1.7% contraction allowed for ductile cast iron, which is a ferrous casting. The pattern was a plate-shaped material for ease of fettling (removal of excess material from castings/knock out, etc) purposes. Figure 1 shows a sketch of the Y- Block pattern for the mould produced

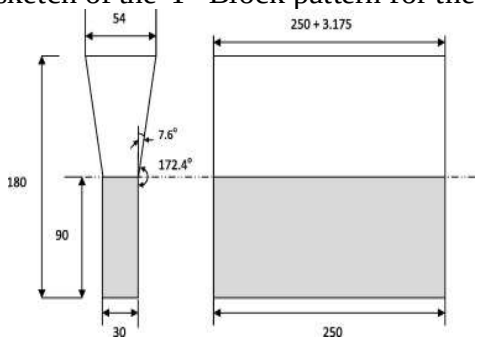

Figure 1 A sketch of the Y- Block pattern for the mould produced

ASTM D7765-18a foundry green sand moulding was used to create the Y-block mould. Clays, moisture, and silica sand were used to make the sand. To guarantee even distribution of the different components throughout the entire sand, a batch muller (a machine that mixes moulding sand to make it suitable for casting) weighing 500 kg each batch with two muller wheels and a number of plough blades was utilised. A maximal binding and enough porosity

were maintained to allow the hot gases to escape, the sand and clay were mixed to give the sand grains a uniform covering of clay. Two types of sands were prepared. The facing and backing sand. The facing sand is the type of sand used before pouring the molten metal, on the surface of the inner part of the mould. It is specially prepared sand from silica sand and clay. To improve the castings' surface polish, it is sprinkled on the interior of the mold chamber. The industrial starch addition was to ensure compactness of the mould since ductile iron has high expansion tendency, the pulverbond (refined and improved clay) addition is to ensure good surface finish to withstand the high temperature of the melt. Often referred to as flour sand, the backing sand supports the face sand. Moulding was used as backing . Coal dustwas added and burns when it comes in contact with the molten metal. Hand moulding technique was used to fill the sand into the moulding flasks since the patterns were of small sizes, then squeezed ramming of the sand was done by applying uniform pressure for both the copes and drags. The patterns were removed and the moulds were covered with appropriate weights placed on top of each and ready for casting. Figure 2 shows the Y- Block moulds

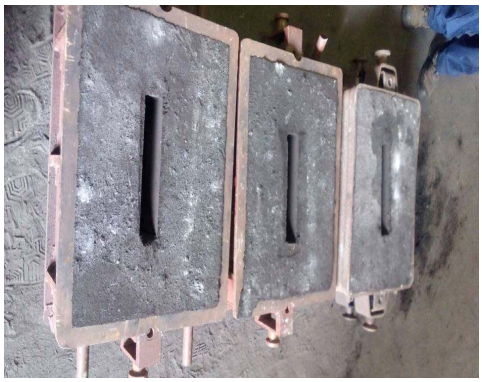

Figure 2 Y- Block moulds

2.2.2 Materials Mould Charge Calculation

Calculations of the poured weight and casting weight of the Y- block pattern

$$Density = {}^{Mass}/_{Volume} \qquad (1)$$

Density of cast iron = 7,800kg/m^3

The Y-block pattern has two shapes, the down part (rectangle) and the upper part (frustrum).

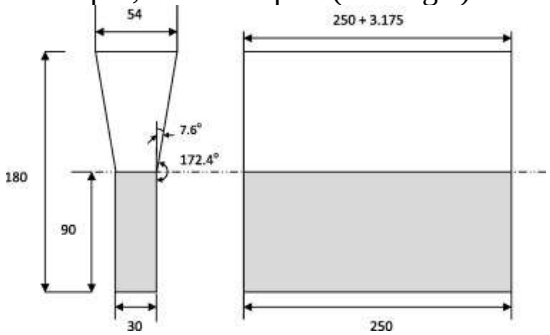

Figure 3 Sketch of the ductile cast iron Y- Block pattern

2.2.4: Samples Preparation

A total of eight Y – Blocks (D_0 – D_{mv}) were cast. The control sample was ASTM A536 (ferritic ductile iron) 65 - 45 -12, then other samples were formed from the control (Do) with the additions of different weight (%wt.) of vanadium and molybdenum respectively.

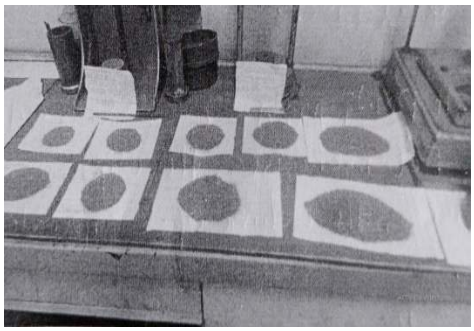

Figure 4 : The ferro-alloys weighed samples (g)

2.2.5 Ductile Cast Iron Production

Figure 5 shows the single track 2500kg induction melting furnace that was used in the ductile cast iron production. This was conducted by treating the grey molten iron with suitable compositions of magnesium alloy which resulted in the precipitation of the graphite in form of discrete nodules instead of flakes, giving the material its characteristic ductility; this process is called "spheroidizing" and it is typically performed just before casting the iron into the desired shape. Steel scraps, ferrosilicon, magnesium ferrosilicon, and carburizer were used to achieve this desired composition.

Figure 5: The single-track induction melting furnace

Ferrosilicon (FeSi) was added in accordance with the charge make-up after graphite coke and steel scrap (CRCA) were charged into the furnace and fully melted at 1450^{o}C. In accordance with ASTM, samples were collected for chemical composition analysis utilising the Optical Emission Spectrometer (OES) to determine the melt conformance. The 1000 kg treatment ladle was transported to the treatment area nearer the moulding floor, and the 600 kg pouring ladle was brought to the furnace to tap 600 kg of the molten metal into. Weighed out for treatments in the melt were magnesium ferrosilicon (Mg-FeSi) and ferrosilicon (FeSi), while a portion of the ferrosilicon (FeSi) alloy was crushed into powder and added as post-inoculation treatment. The different alloying elements (FeV, Femo) were added to the melt . The mg -fe - si was transferred into ladle and some mild steel filings were poured on it to cover the ferroalloy to prevent its direct contact with the molten metal (this was done to reduce the spontaneous and violent reaction of the molten metal and the magnesium ferrosilicon). The melt (600kg) was transferred into the ladle (1000kg) and there the reaction took place. Subsequently, the melt was promptly moved to the 600 kg pouring ladle, in which the ground ferrosilicon powder was added (pre-inoculation or early). Slag was removed and the moltem metal were cast into the different moulds. However, the pulverised ferrosilicon was injected simultaneously prior to the molten metal being poured into their respective moulds. The molten metal was cast into the moulds within 7 minutes of touching the magnesium ferrosilicon (Mg-FeSi) inside the ladle; beyond that, the melt progressively

transformed into a grey cast iron (flakes form). Solidification occurred within the 7 minutes time in order to ensure nodule formations in the microstructure and also more nodule count. Figure 6 shows the mould of cast sample

Figure 6 : The mould of cast samples

2.3 Method/Procedures/Production of the False Wall (Canarium Schweinfurthii) Fruit Oil

For the purpose of carrying out this research study, 25 liters of the fruit oil (False Wall) was used. This oil was processed mechanically (press cold method) in Vom Jos, Plateau State, a village in Jos South Local Government Area, Nigeria where the oil was enhanced in abundance. Figures 7 and 8 shows the raw fruits and extracted oil .

Figure 8: Raw fruits (false wall fruit oil)

Figure 9: Extracted oil from raw fruits

2.4 Determination of the Chemical Characteristics of the False Wall (Canarium Schweinfurthii) Fruit Oil

The physico - chemical analysis/characteristics of the raw oil (flash point, saponification value, density, acid value, viscocity, etc) were done at No. 70 Udoka Housing Estate Awka, Anambra State, Nigeria. They were all done at room temperature of 28^0C. Table 7: Physico-chemical characteristics of the false wall oil.

Table 7: Physico-chemical characteristics of the false wall oil

OIL	Free fatty acid (%)	Saponification value (mg/KOH)	Iodine value (%)	Density (g/mol)	Peroxide value (mleg/kg)	Boiling point (^{0}C)	Acid value (%)	Viscocity (pa.s)	Flash point (^{0}C)	Temperature (^{0}C)
False Wall	7.547	8.135	31.22	0.85	38.6	190	15.147	1.5660	290	28

2.4 Salt Bath Furnace

The workpieces are subjected to experimental process utilizing the salt bath furnace, which was a metal container filled with fused salts. Salt-based substances are present in the furnace. Salt mixture was chosen. The temperature of a salt bath boiler was set at 1500 ^{o}C . the salts serve as resistors for the passage of current in fused state of excellent resistors and was utilized to heat up the material . The treated material's great wear resistance was ensured by this hardening procedure. The material was first heated to an austenitizing temperature of 850^{o}C to 950^{o}C. After that, the material was cooled in a bath of molten salt that was maintained at an austempering temperature at 450^{o}C at constant and isothermal levels. The outstanding temperature homogeneity of the salt bath furnace guarantees optimum thermal transfer to the work piece. For homogeneity reasons, heat transfer process was completed with shorter dwell durations than in chamber furnaces. A mixtures of nitrate-based salts (KNO_3 and $NaNO_3$) were used at 300^{0}C which was dependent on the salt characteristics.

2.5 Experimental Heat Treatment Procedures

This researched work was based mainly on the alloyed oil austempered heat-treated ductile cast iron samples with salt as a standard austempering method for comparisons. The heat treatment was performed according to ASTM A897-90 standard specification for ADI castings. After being identified, the samples were put in a heat treatment furnace and heated to 920 °C, which dissolved nearly all of the carbon in the austenite. To ensure carbon homogeneity for all of the heat-treated cast samples, the samples were immersed in the furnace for one hour. As a common austempering technique, a combination of potassium nitrate (KNO_3) and sodium nitrate ($NaNO_3$) salts was employed in the salt bath furnace for the austempering heat treatment, while a locally sourced oil (false wall oil fruit) also known as canarium schweinfurthii/borium fistuta oil was also used to compare their effects at the same operated/quenched conditions.

2.6: Mechanical Property Tests

The produced samples were subjected to mechanical property tests, which include tensile (tension), compression, flexure, impact, and fatigue. The tested material specimen's show resistance to stretching and ascertain their mechanical characteristics, such as tensile strength, yield strength, and ductility basically, determining how much stress a material can bear before breaking when pulled apart a pulling force is applied to the specimen.

3.6.1 Tensile Test

The ASTM E8/E8M standard test procedures for tensile testing of metallic materials were used to conduct the tensile test. Before loading the specimens into the Instron machine, the parameter of gauges were entered into the computer system that was connected to the machine where a precise portion of the specimen's elongation were determined. The specimen's length, diameter, and tension speed. The "speed of tension" of the materials were rated at which forces were applied to stretch the materials , the rate at which the material was pulled apart. Tensile tests were performed after the specimens were loaded into the

Instron machine. The load-deflection curve was displayed visually on the computer screen after the data was electronically captured in text files. Elongation to failure, 0.2% proof strength, and ultimate tensile strength were measured. The average value was calculated using three samples. Figures 10 and 11 shows the sketch of the tensile test sample dimensions (mm) and Tensile test samples

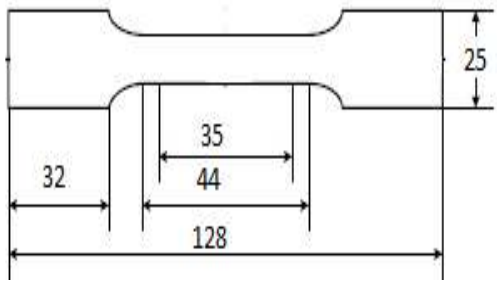

Figure 10: Sketch of the tensile test sample dimensions (mm)

Figure 11: Tensile test samples

2.6.2: Impact Test

In accordance with ASTM E23 (ASTM standard of impact test for metallic materials), these tests were carried out. At an angle of 150^{o}C, the striking hammer was allowed to fall freely. Half of the V-notch was inside the vice and half was above the top surface, facing the striking hammer. The striking harmer was brought to its topmost position and the dial scale was set to 300j (maximum energy), the hammer was released from its height to fall under gravity to break the sample. As the pendulum hit the sample, the sample was broken from the v-notch. The caliberated scale, which showed the material's resistance to load before fracture, was used to calculate the energy absorbed by the specimen.Figures 12 and 13 show the sketch of impact test and the Impact test samples sample dimensions (mm)

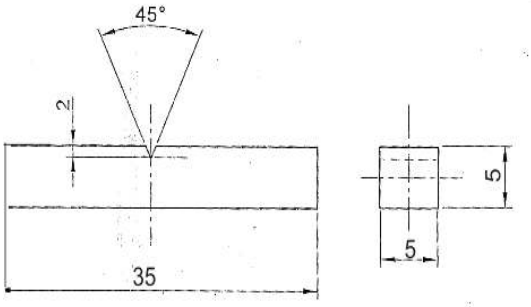

Figure 12: Sketch of impact test sample dimensions (mm)

Fig 13: Impact test samples

2.6.3: Hardness Test

The hardness test indicates the resistant on material's surface is to cutting, scratching, and abrasion. It is a form of resistance to identification. The ASTM E10 standard procedure for determining the Brinell hardness of metallic materials was followed in this process. Samples were ground to achieve a flat surface, then the machine was calibrated by placing standard materials to test their hardness. This was done to eliminate erroneous results. The diamond balls were placed (for ferrous materials) and the machine records readings in HRB.

Plate 15: Hardness test samples

2.7 Metallographic Examinations

Metallographic examinations were carried out in all the produced ductile cast iron samples. Metallographic sample preparation was performed according to ASTM E3 – 11(2017) standard guide for preparation of metallographic specimens. Specimen samples were cut, sectioned and mounted using a semi – automatic Buehler hot mounting press. The thermosetting bakelite powder was poured into the cylinder, locked and heated up to 200^0C after which the heater was turned off as the pressure knob was engaged to 150psi. The heater commenced for another 15 minutes before it was cooled down and the specimens removed from the cylinder to proceed with the coarse grinding using LECO BG20 coarse grinding wheel with 120 grits on a silicon carbide impregnated abrasive clothe then to 180 grits to achieve a smooth and bevelled free surface. Surface medium and fine grinding operation were performed using a semi automatic grinding wheel. The polishing operations were done on a mechanized polishing wheel using a sylvethe clothe and successive alumina (Al_2O_3) polishing paste; 5-micron meter, 1 micron meter, 0.5-micron meter, and 0.05-micron meter for final polishing. Etching was done using 2% Nital (2ml nitric acid in 98ml ethanol), then the samples were dried and ready for microscopy examinations. The prepared samples were avoided by not touching them with their hands and instead they were stored in desiccators. The optical microscopy was also done according to ASTM E3-11 (2017) a standard guide for the preparation of specimens. The specimen was placed on the sample holder of a computer-controlled Leco Olympus GX 51 microscope. The parameter was set, images were captured and stored in the image archives.

3.8: Trial Tests Gears Samples (Spur Gear)

Spur gears are cylindrical, toothed parts used in cylindrical machinery to transfer mechanical motion and control torque, power, and speed. These gears are affordable, sturdy, and reliable, and they provide a positive, constant speed drive to support common industrial applications. They go by many other names, such as spur wheels, spur gearing, straight gears, and straight-cut gears. The gear samples that were machined from the Y-Block cast samples before the heat treatment procedures are shown in the specimens .Figures (16).(a) & (b) shows the machined ductile cast iron spur gear samples (a) Molybdenum and (b) Vanadium

) Molybdenum (b) Vanadium

Figure 16: Machined ductile cast iron spur gear samples

3.0 RESULTS AND DISCUSSION

3.1 Chemical Compositional Analysis

The compositional analysis of the unalloyed and alloyed results for this research work are as indicated in Table 8 while Plates 16 - 17 depict the micro-structural analysis.

Table 8: Chemical Compositions of the unalloyed and alloyed Ductile Cast Iron samples

SAMPLE	Fe	C	Si	Mn	P	S	Mg	Vn	Mo
D_o	92.98	3.59	2.76	0.145	0.016	0.002	0.041	0.019	0.034
D_{v1}	90.60	3.39	2.30	0.813	0.005	0.030	0.027	0.048	0.033
D_{v2}	90.42	3.29	2.11	0.255	0.020	0.046	0.024	0.120	0.038
D_{v3}	90.55	3.17	2.43	0.227	0.044	0.045	0.023	0.160	0.035
D_{m1}	93.00	3.65	2.22	0.360	0.005	0.002	0.031	0.130	0.021
D_{m2}	90.72	3.48	2.47	0.210	0.010	0.043	0.027	0.190	0.020
D_{m3}	91.10	3.50	2.29	0.296	0.020	0.043	0.029	0.287	0.017
D_{mv}	92.17	3.44	2.31	0.160	0.023	0.038	0.034	0.044	0.098

It was observed that their respective carbon content was sufficient enough for graphitization to occur and reduced as the alloying elements increased which showed that vanadium and molybdenum were strong carbide formers(Ingole et al, 2012). The silicon content in the melt was within the range of 2.11 to 2.76wt%, which on the other hand promoted graphite formation, which was adequate enough to prevent melt chill and also sufficient to have facilitated nodule count and nodularity of the cast specimens, thus reduced carbides formation, this is in agreement (Kiani & Rashid, 2009). The residual magnesium in the ductile cast iron was within 0.023 to 0.041 which was sufficient enough to produce nodules in the melt but it was observed that the magnesium wt. % decreased(0.04-0.023) as the alloying elements (vanadium and molybdenum) increased. This was due to the formations of complex iron compounds inclusion such as magnesium sulphide (MgS), irons of magnesium, vanadium, molybdenum Fe(Mg, Vn, Mo) and magnesium sulphate ($MgSO_4$) which resulted in hampering nodularity as the alloying elements weight percentages increased (Marcin et al, 2017). The carbon equivalent(CE) of the controlled sample (D_o) was sufficient enough to produce high nodularity and nodule count which were evenly distributed throughout the matrix. As the samples were being alloyed with such strong carbide formers like vanadium and molybdenum, the carbon equivalent (CE) decreased to about 4.0% as those alloying elements reacted with the free carbon to form carbides (Soedarsono W.J *et al,* 2011).

3.2: Micro-structural Analysis of the non-heat treated Unalloyed and Alloyed samples

Plates 17 - 24 depicts the micro-structural features of the non-heat treated (virgin) Unalloyed and Alloyed Ductile Cast Iron samples produced.

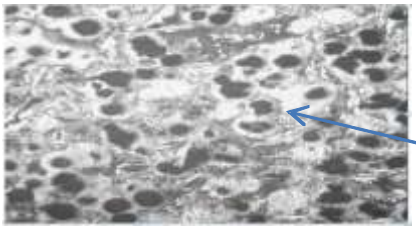

Plate 17:As-cast unalloyed (D_0)

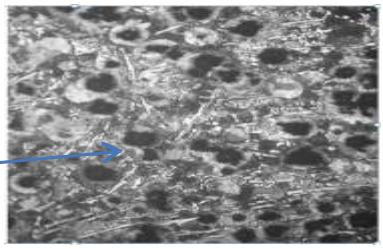

Plate 18:As-cast alloyed (D_{v1})

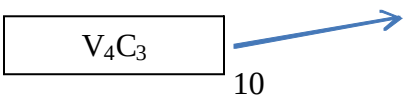

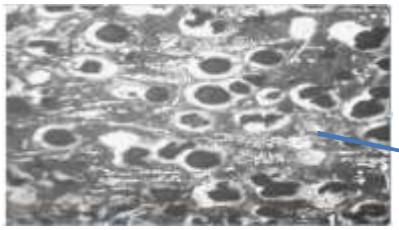

Plate 19:As-cast alloyed (D_{v2})

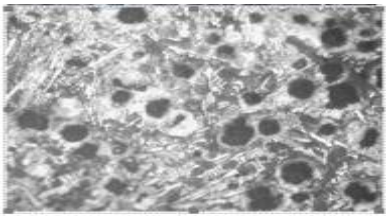

Plate20:As-cast alloyed (D_{v3})

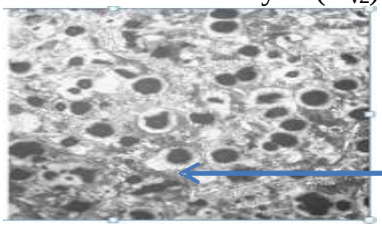

V_4C_3

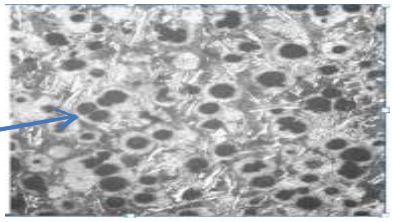

Plate 21: As-cast alloyed (D_{m1})

Plate 22:As-cast alloyed (D_{m2}

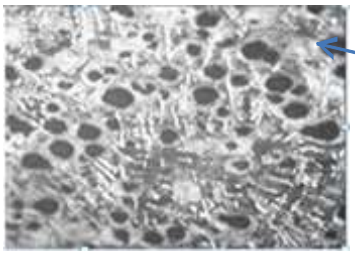

Mo_2C

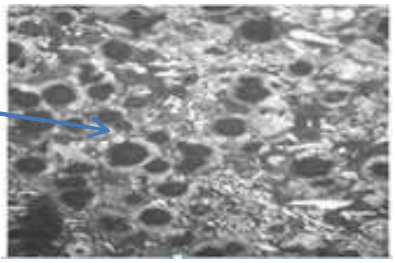

Plate 23: As-cast alloyed (D_{m3})

Plate 24: As-cast alloyed (D_{mv})

When eutectic carbide forms in an alloy, a fine, interpenetrating microstructure of carbide particles within the metal matrix is created, resulting in improved wear resistance and hardness due to the hard carbide phase acting as reinforcement within the softer metal matrix, while potentially impacting on other properties like machinability depending on the specific alloy composition and carbide morphology; essentially, the alloy becomes harder and resistant to wear and abrasion. On the improved strength, depending on the size and distribution of the carbides, the alloy's tensile strength can also be positively impacted upon. In their potential for reduced machinability, a high volume of the fine carbides can make the alloy more difficult to machine due to the increased tool wear. In their microstructure, the eutectic carbides typically appear as small, uniformly distributed particles with a characteristic lamellar or rod-like structure, creating a very fine-grained microstructure. In their solidification process, the microstructure formed during the final stage of solidification when the alloy reaches the eutectic temperature, where the liquid rapidly transforms into a mixture of the metal matrix and carbide particles simultaneously. In their alloying elements, the specific type of carbide formed depends on the alloying element present, with common examples including M2C and M6C carbides (where M represents a transition metal like Mo, Cr, Vn, etc). Areas of applications include: In high speed steels, the eutectic carbides are intentionally added to high-speed steels to maintain hardness at elevated temperatures during cutting operations. In wear resistant components, parts like bearings, gears, and cutting tools often utilize alloys with eutectic carbides to resist abrasive wear. In cast irons, white cast iron owes its high wear resistance to the presence of eutectic carbides.

3.3 As-cast Unalloyed (Do) Sample

The microstructure of the as-cast (plate D_0) structure displayed a typical bull eye structure with ferrite (white ring) surrounding the graphite nodules in a pearlitic matrix with a little intercellular carbide.

3.3.1AlloyedVanadium (0.05-0.15wt%) Samples

A reduced ferrite phase and nodule count were observed in the alloyed vanadium as the weight percent increased, thereby promoting the pearlite phase. This was suggested to be as a result of the carbide forming alloying element in the ductile cast iron. From the alloyed vanadium microstructure, there was an increased crystal structure of vanadium carbide (V_4C_3) forming a rich vanadium phase (plate Dv_3) thereby promoting eutectic carbide formation (the process where, within a metal alloy, tiny, uniformly distributed carbide particles precipitate simultaneously with the surrounding metal matrix during solidification, occurring at a specific temperature known as the eutectic point, creating a characteristic microstructure with fine, interlaced carbide phases; essentially, it is the simultaneous crystallization of two different phases (metal and carbide) from a liquid solution at a fixed temperature, often observed in high-carbon steels and cast irons. As mentioned above, the resulting microstructure typically features fine, needle-like carbide particles embedded within the matrix, giving the material unique mechanical properties.

3.3.2 Alloyed Molybdenum (0.1 - 0.3wt%) Samples

Molybdenum promoted the ferrite phase as the content increased from 0.1wt% to 0.3wt%. The microstructure showed more of the ferrite phases as compared to the unalloyed as-cast ductile iron. As the molybdenum concentration rose, the impact energy rose as well, indicating an increase in toughness. As the molybdenum level rose, the microstructure displayed an increase in the ferrite phase and nodule count. When it reached 0.3wt%, more carbide forms were observed, indicating that it had progressed to a ductile to brittle and ferrite to pearlite phase transition stage. A hard carbide phase of molybdenum carbide (Mo2C) is shown by the asymmetric needle-like white structure.

3.3.3 Alloyed Combinations of Vanadium (0.05wt%)/Molybdenum (0.1wt%) Samples

The alloyed combinations of vanadium and molybdenum (Dmv) showed an excellent property of lower mechanical properties as when compared to the as-cast unalloyed (D_0) where elongation was increased by 20%. The microstructure revealed more pearlite but scanty carbide phase which suggested that the combination of the rich vanadium and molybdenum phases present dissolved the carbides leaving behind little intercellular carbide.

3.4 Nodule Count and Nodularity

The nodule count and nodularity for all the ductile cast iron samples produced were as shown in the Table 9 Nodule Count/Nodularity

Table 9 Nodule Count/Nodularity

S/N	Samples	Nodule count (Nod/mm^2)	Nodularity (%)
1	D_0	89	93
2	Dv_1	115	81
3	Dv_2	98	91
4	Dv_3	93	85
5	Dm_1	104	90
6	Dm_2	124	91
7	Dm_3	147	89
8	Dmv	130	87

3.5: Mechanical Characterization of the Non-Heat-Treated Unalloyed and Alloyed Samples

The mechanical characterization of all the unalloyed and alloyed steels that did not undergo the austempering heat treatment. Table 10 shows the as-cast ductile iron (D_0) meeting the standard ASTM A536 properties of 406MPa tensile strength, 12.5% elongation, 170BHN hardness and impact energy of 16.32J. Figures 17 and 18 show the Graph of the as-cast molybdenum alloyed and the Graph of the as-cast vanadium alloyed.

Table 10: Summary of the Mechanical Property Test of the as-cast Unalloyed (Do) Specimen

Specimen	Tensile (MPa)	Hardness (BHN)	Impact (J)	Elongation (%)
Do	406	170	16.32	12.5

(a) As-Cast Molybdenum Alloyed:

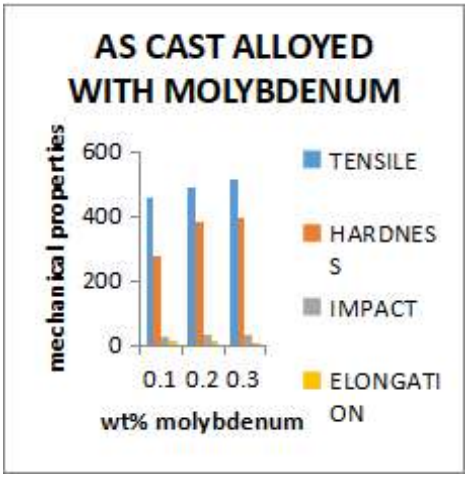

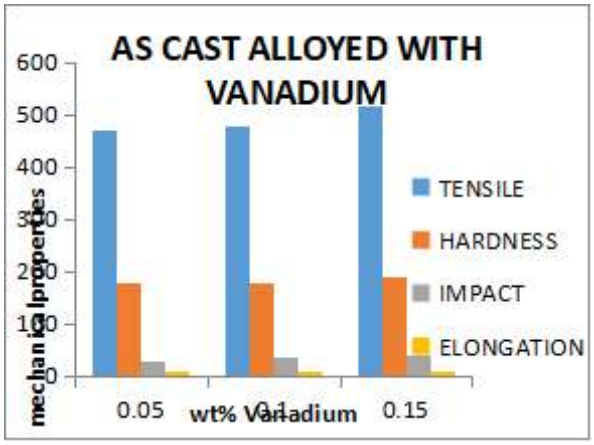

Figure 17: Graph of the as-cast molybdenum alloyed Figure 18: Graph of the as-cast vanadium alloyed

From the mechanical properties of molybdenum content of 0.1wt%-0.3wt% %), molybdenum slowed down the transformation start to pearlite by increasing the eutectoid temperature (high pearlite). The 0.1-0.3wt% molybdenum acted as ferrite stabilizer thereby having improved the tensile strength, hardness and impact properties in the as cast alloyed condition as listed respectively 461.08MPa - 517.86MPa, 275BHN - 397BHN, 27.76J - 31.76J while there was a slight decrease in the elongation from 11.16% - 8.93% and shown below in Table 11. The as cast alloyed samples showed an increase in properties as the molybdenum content increased from 0.1 - 0.3%. This can be validated by the study by (Farahat 2018) on the impact of molybdenum in ductile iron. A study (Avila et al, 2015) examined how molybdenum affected the microstructure of nodular cast iron. The improved tensile, hardness, and impact properties, along with decreased elongation, in the as-cast condition of the specimen, were due to the presence of a high pearlitic structure in the alloy and a high volume of molybdenum-carbide formed during solidification. Table 11 shows the summary of the mechanical property test of as as-cast molybdenum alloyed.

Table 11: Summary of the Mechanical Property Test of the as-cast Molybdenum Alloyed Specimen

Specimen	Tensile (MPa)	Hardness (BHN)	Impact (J)	Elongation (%)
Dm1	461.10	275	27.76	11.16
Dm2	492.30	382	28.9	10.2
Dm3	517.86	397	31.76	8.93

3.6 As-Cast Vanadium Alloyed:

From the mechanical properties shown in Figure 4.1 above, the strength, impact, and hardness increased linearly, while elongation decreased, as the vanadium content increased. Vanadium had a strong tendency to promote eutectic carbide (M_4C_3) formation as it is a good carbide stabiliser. It modified the solidification of the metastable austenite/cementite system, thereby forming a vanadium-rich phase, usually referred to as the second phase during solidification. This second phase was suspected to be the eutectic carbide (V_4C_3), which comprised about 75 - 80% present in a coarse form. Tensile property increased from 468.9MPa (0.05wt%V) to 516.65MPa (0.15wt%V). This was because the volume fraction of graphite in the material, or a measure of the proportion of graphite in the material (ie a way to express the composition of the mixture) reduced at the expense of the increased eutectic carbide (V_4C_3). This was responsible for the increased hardness as suggested by (Rezvani et al, 1997).

The decrease in elongation is attributed to the second phase (vanadium carbide), which acted as crack initiation sites for both brittle and ductile types of fracture. As vanadium content increased to 0.15wt%, volume fraction of the second phase increased with increased pearlite fraction, thereby promoting sites for crack and reduction in ductility because graphite nodule count decreased as carbide increased, as suggested by (Rezvani et al, 1997. The per cent elongation decreased from 11.06%-8.7% as the vanadium content increased to 0.15 wt% due to the presence of coarse vanadium carbide in the intercellular region on the fracture surface, as suggested by Honeycombe and Barton. This should be considered as a factor which decreased the total. Table 12 gives a summary of the mechanical property test of the as-cast vanadium alloyed specimen

Table 12: Summary of the Mechanical Property Test of the as-cast Vanadium Alloyed Specimen

Specimen	**Tensile (MPa)**	**Hardness (BHN)**	**Impact (J)**	**Elongation (%)**
Dv1	468.9	177	28.36	11.06
Dv2	477.5	179	37.47	10.5
Dv3	516.7	191	38.90	8.7

3.5.1 Alloyed Combinations of Molybdenum/Vanadium

Low alloyed combinations of molybdenum and vanadium contributed immensely in enhancing the mechanical properties as compared with the unalloyed as-cast (Do) sample, although there was a decrease in the percentage elongation. Table 12 shows the summary of mechanical property test of the combinations of molybdenum (0.1wt%)/vanadium (0.05wt%) alloyed specimen

Table 12: Summary of Mechanical Property Test of the combinations of Molybdenum (0.1wt%)/Vanadium (0.05wt%) Alloyed Specimen

Specimen	Tensile (MPa)	Hardness (HBN)	Impact (J)	Elongation (%)
Dmv	491.04	278	28.18	11.31

3.5 Microstructural Analysis/Mechanical Characterization of the heat-treated Unalloyed and Alloyed Specimens in both media (Oil and Salt)

3.6: Unalloyed/Control (Do) heat-treated Specimens

Plates 25 - 32, show the microstructures of the austempered unalloyed ductile cast iron (Do) These reveal the microstructures of the produced austempered unalloyed (Do/control) cast specimens from the two austempering media (oil and salt).

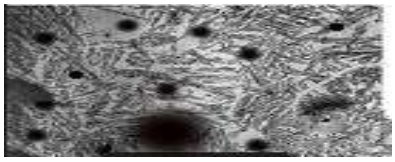

Plate 25 :Unalloyed(Do) 1hr Oil

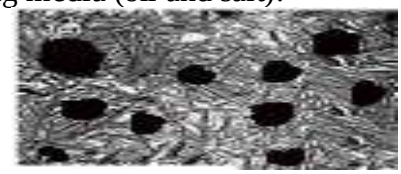

Plate 26: Unalloyed (Do) 1hr Salt

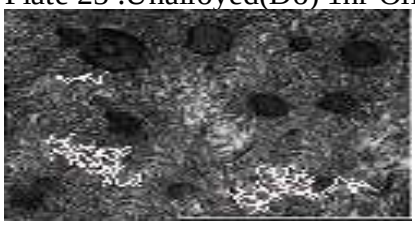

Plate 27:Unalloyed (Do) 2hrs Oil

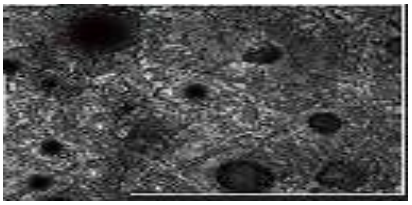

Plate 28:Unalloyed (Do) 2hrs Salt

Plate 29 : Unalloyed (Do) 3hrs Oil

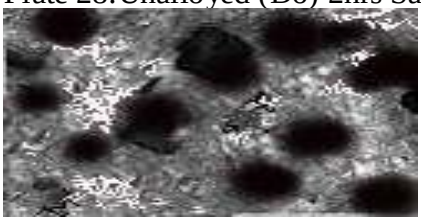

Plate 30: Unalloyed (Do) 3hrs Salt

Plate 31: Unalloyed (Do) 4hrs Oil

Plate 32: Unalloyed (Do) 4hrs Salt

The pearlitic matrix changed into austenite and some ferrite, which were still impacted by the austenitizing temperature, and the microstructures were composed of two phases that coexisted as ferrite and austenite. The austenite began to develop through the ferrite grains after being collected at the grain boundaries. A pearlitic matrix overlaid with carbon-enriched austenite was the outcome of this growth. While the termination of the ferrite grain development complicates the later diffusion of carbon, further nucleation of the austenite at the primary ferrite's grain boundaries enriches and saturates the austenite with carbon. (Mao et al. ,2025). As the austempering time increased, the matrix transformed to a more ferritic phase for both salt and oil media, which contains ausferrite, carbon-enriched austenite, retained austenite, and graphite nodules. The volume fraction or percentage by volume (expressing the composition of the mixture) of these components varies as the austempering time varies. (Putatunda, S. K. 2001). Tiny acicular ferrite gathered, nucleated, and formed

around the nodules during the isothermal heat treatment process. This was caused by the high energy potential and the subsequent expansion of the ferrite platelets, which resulted in the creation of carbon-enriched austenite. Austempering changed the ferritic-pearlitic matrix to a combination of acicular ferrite while retaining austenite. (Konca *et al*, 2017).

At 1 hour austempering time, there was a large volume of retained austenite and a lower amount of acicular ferrite. At 3 hours austempering time, the retained austenite transformed into more needle-like acicular ferrite with pearlitic matrix while the carbon-enriched phase remained. Beyond 3 hours of the austempering time, the acicular ferrite reacted to form more carbides, while the carbon-enriched phase transformed into complex carbides which resulting to poor ductility and low toughness but improved tensile strength and hardness. During the austempering heat treatment, the austenite phase, which was indistinguishable from the ferrite phase, is replaced by the bainitic ferrite phase. This occurred as a result of the retained austenite's excess carbon distribution, which stabilized while cooling to room temperature without running the risk of turning into martensite. The absence of martensite in the microstructures suggests that the austempering schedule was chosen correctly. The two austempering media do the same thing but the oil takes more time to achieve the same result as the salt. This was because the oil has a lower heat capacity, which resulted in the white phase being suggested for an unreacted austenite phase. while Figures 19 - 22 show the mechanical property tests.

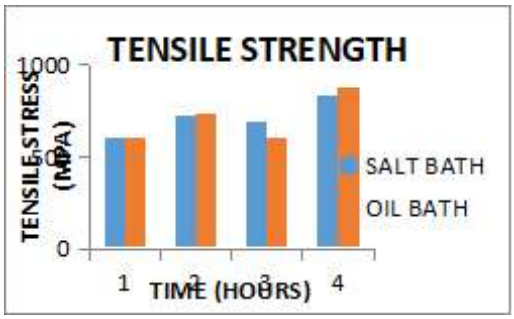

Figure 19: Graph of the Unalloyed (Do) heat treated Tensile Strength property test specimens vs Time variations

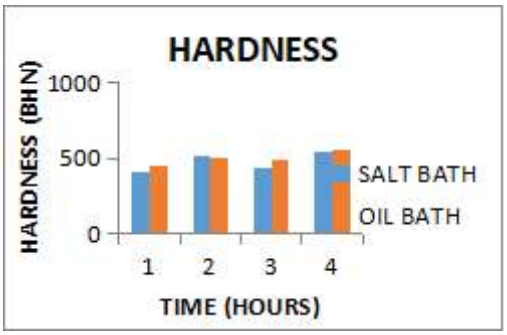

Figure 20: Graph of the Unalloyed (Do) heat treated Percentage Elongation property test specimens versus Time variations

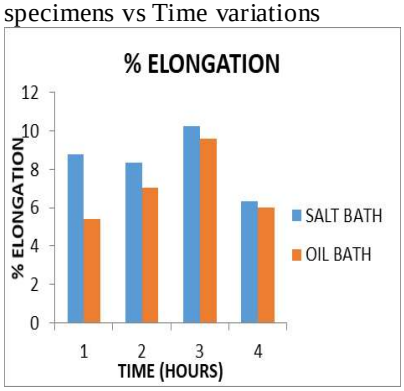

Figure 21: Graph of the Unalloyed (Do) heat treated Hardness property test specimens versus Time variations

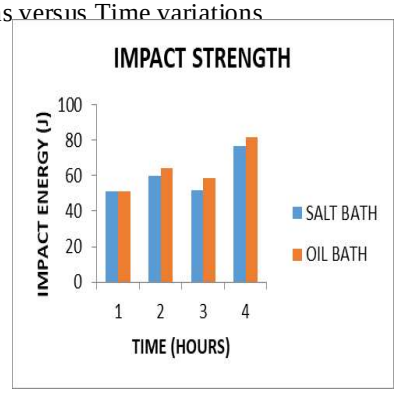

Figure 22: Graph of the Unalloyed (Do) heat treated Impact Strength property test specimens versus Time variations

From Figures 19 - 22 above, the tensile stress increased at 1 hr and 2 hrs due to the presence of banitic ferrite, retained austenite and some small amount of martensite. At increased austempering times, the "martensite" disappears, this was because at such short austempering times, the carbon content was insufficient to retain the stability of the retained austenite and consequently, as Olivera recommended, it was changed to martensite. E et al. (2006) studied ADI alloyed with copper. At short austempering time, there was significant amount of brittle

fracture caused by the presence of martensite in the structure; this is because the stage 1 reaction in austempering heat treatment produced high carbon austenite (martensite) and ferrite which caused an increase in the tensile stress up to 724.4MPa and 735.26MPa respectively for salt and oil medium at 2hrs. After the 2hrs treatment, the tensile, hardness and impact energy decreased a little between 3 to 4hrs while the elongation increased because the stage 1 reaction is completed and better properties were achieved at such processing window as suggested by M. Ramadan et al, 2006 in their study of influence of graphite nodularity on microstructure and processing window of 1.5%Ni-0.3%Mo austempered cast iron. At the austempering time of 4hrs, the tensile stress, hardness and impact increased for salt medium as follows: 837.38MPa, 545BHN, 76.52J respectively and oil medium as follows: 881MPa, 555BHN, and 81.82J respectively. This was because the stage II reaction in the austempering process was as a result of the longer austempering time, which resulted in further decomposition of high carbon austenite into ferrite and carbide, as suggested by(Ramadan et al, 2006) in their study. The elongation increased to 10.25% and 9.6% as the austempering time reached to 3hrs and further reduced to 6.34% and 6.03% respectively for salt and oil medium because of the carbide formation. This is in line with (Sandeep, 2012), ()Lawrence, 2011, (Elliot & Yazdani, 1999)as seen from the figures above showcasing the tensile stress, elongation, hardness and impact strength increasing at the start of the austempering reaction then decreased and later increased due to the high carbon enriched austenite transformed into bainitic ferrite and ε-carbide. The ε-carbide is responsible for the brittle fracture/failure and low elongation in metals.Table 13 show the summary of the mechanical property test on the austempered unalloyed Control (Do) Specimens versus Time variations.

Table 13 Summary of the Mechanical Property Test on the Austempered Unalloyed Control (Do) Specimens versus Time variations

Do	**SALT**				**OIL**			
	1hr	2hrs	3hrs	4hrs	1hr	2hrs	3hrs	4hrs
Tensile (Mpa)	602.7	724.4	689.9	837.38	603.9	735.26	602.39	881.10
Hardness(BHN)	415	521	432	545	450	505	493	555
Impact (J)	51.28	60.05	51.82	76.52	51.08	64.08	58.90	81.82
Elongation (%)	8.8	8.37	10.25	6.34	5.42	7.02	9.60	6.03

4.5.2 Molybdenum Alloyed (Dm_1 - Dm_3) Heat Treated Specimens

Molybdenum is the most potent (possessing strength, very powerful) hardenability agent in ADI and may be required in thick sections to prevent the formation of pearlite. This element is also used to increase austemperability in ductile cast iron. Molybdenum above 0.3 wt% in a ductile iron causes segregation in the eutectic cell boundary during solidification, which leads to an unsuitable matrix for austempering. Also, due to its carbide-forming ability, the amount of carbide formation increases in the microstructure as the molybdenum content increases. Molybdenum presence decreased the free carbon content in the parent austenite, as it does not delay austempering with little or no effect on the processing window changes. (Amir Sadighzadeh, 2015). Molybdenum-carbides are very stable and hardly dissolved during the austenitization, such that it delays the stage II austempering reaction. Plates 33 – 38 show the microstructures of the austempered molybdenum alloyed ductile cast iron (Dm_1).

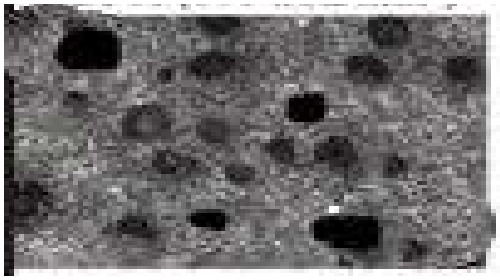

Plate 33 Alloyed (Dm1) 1hr oil

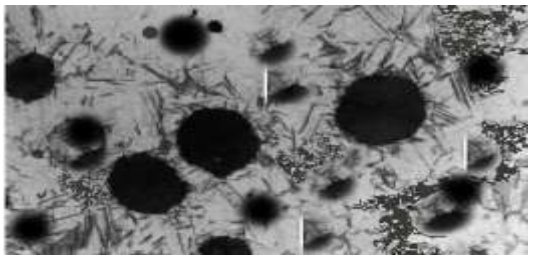

Plate 34: Alloyed (Dm1) 1hr salt

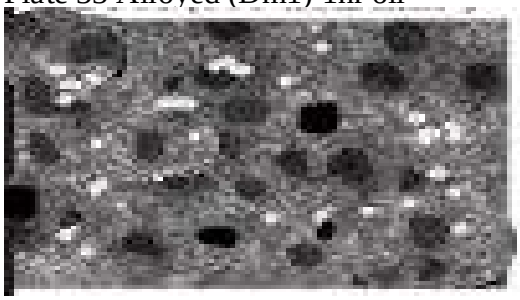

Plates 35: Alloyed (Dm1) 2hrs oil

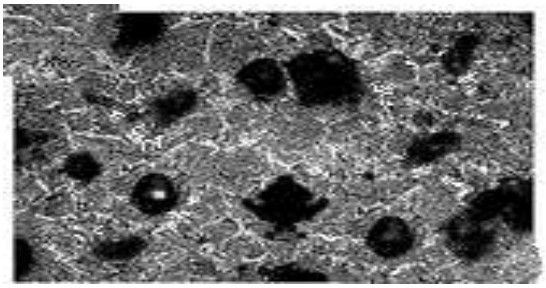

Plate 36: Alloyed (Dm1) 2hrs salt

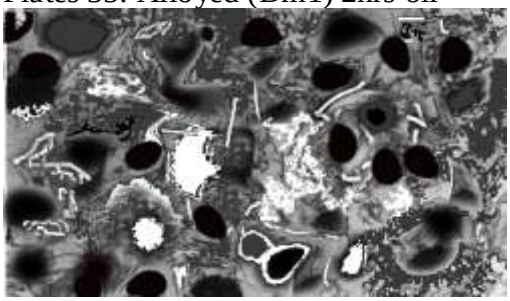

Alloyed plate 37: (Dm1) 3hrs oil

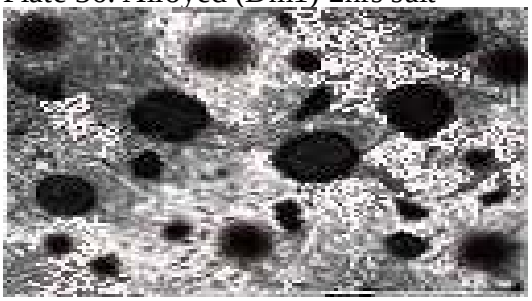

Alloyed Plate 38: Alloyed (Dm1) 3hrs salt

Austempering at 1 hr alloyed with molybdenum consists mainly of acicular ferrite in a stabilized high carbon ausferrite matrix, carbide and graphite nodules. At 1hr austempering, the stage I reaction begins and as the austempering time increases to 4hrs, the microstructure moves from ferritic to pearlitic matrix while the carbide volume fraction increased up to 2hrs then reduced at 3hrs. this may be as a result of complete disolution of the carbides formed with the alloying element. (stage II reaction). At 4 hours, there was increased mechanical properties and complex secondary carbides because of the start of stage II reaction with increased nodule count in the microstructure. Transformation occurs when formation of carbides sets in from the carbon enriched austenite which weakens the properties of the sample and high nodule count (Soedarsono et al, 2011). Table 14 showed the mechanical properties tests (tensile, elongation, hardness and impact values for the salt and oil austempering medium with austempering times variation (Dm_1). At molybdenum of 0.1wt% (Dm_1), there was an increased tensile strength from 1-2hrs at 748.3MPa to 779.1MPa, 795.4MPa to 886.7MPa for salt and oil respectively then decreased to 706.2MPa and 776.6MP at 3hrs before it increased to 863.5 and 985.6MPa at 4hrs. This was caused by the stages of austempering and formation of martensite at the first stage then ε-carbide at the second stage as suggested(Yazdani & Elliot, 1999). Also the salt bath showed a lower tensile strength, hardness and impact energy values with higher elongation while a slight increase was noticed in that of the oil medium. These were the` same for hardness and impact. At increased molybdenum content up to 0.3wt%, tensile strength, hardness and impact increased progressively for salt and oil medium from austempering time to 2hrs then a slight decrease with increased elongation after which it increased at 4hrs. This was because of the martensite formation during the stage I austempering and complex molybdenum-carbide

and ε-carbide formation during the stage II reaction. Figures 23 -26 show the graphs of molybdenum alloyed (Dm_1) heat treated property tests versus time variations

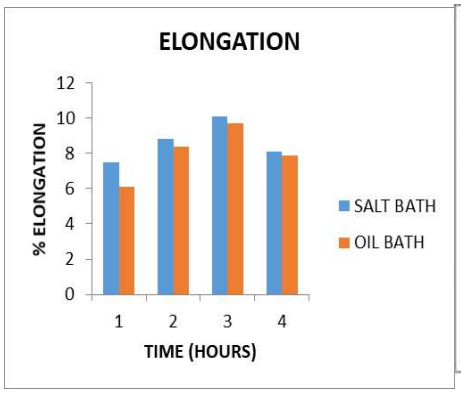

Figure 23: Graph of the Molybdenum Alloyed (Dm1) heat treated Tensile Strength property test heat treated specimens versus Time variations.

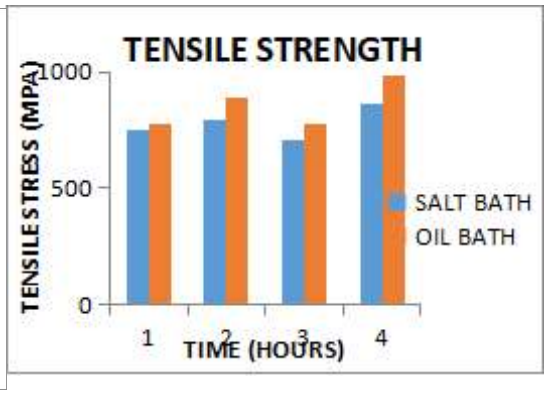

Figure 24: Graph of the Molybdenum Alloyed (Dm1) % Elongation property test specimens versus Time variations

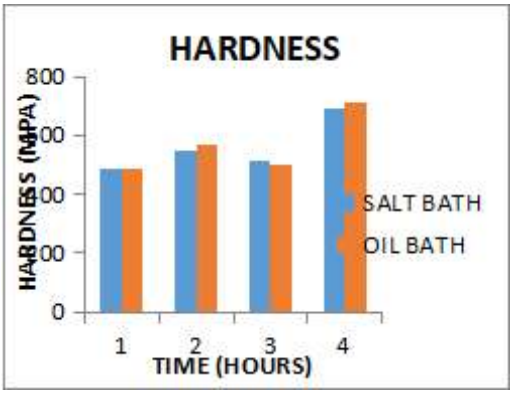

Figure 25 Graph of the Molybdenum Alloyed (Dm1)heat treated Hardness Property test specimens versus Time variations

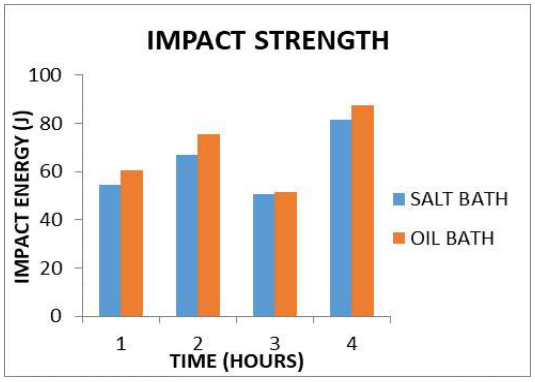

Figure 26: Graph of the Alloyed (Dm_1) heat treated Impact Strength property test specimens versus Time variations

3.6: Physio-Chemical Characteristics of the False Wall (Canarium Schweinfurthii) Fruit Oil

Table 15 displays the findings of the physio-chemical properties of the fruit oil utilised for the false wall in this investigation. The oil is of the none-drying kind since the iodine value of 31.22% is less than the required value of 100% for the salt bath (Ayo et al, 2007). The amount of reactive radicals in the fake wall fruit oil was low, according to the value. Additionally, it demonstrated how stable the coating of fatty acid molecules that developed on the metal surface was (Hassan,2003). Generally speaking, an oil's degree of unsaturation and propensity to experience oxidative rancidity increase with its iodine value. When an oil's unsaturated fatty acids combine with atmospheric oxygen, a chemical breakdown or decomposition takes place, producing volatile chemicals such aldehydes. This phenomenon is known as oxidative rancidity and ketones, resulting in an unpleasant odour, off flavours, smelly and taste, essentially making the oil “rancid” (distinctly unpleasant or distasteful: offensive) this process is accelerated by factors like heat and light, and essentially a free radical chain reaction where oxygen molecules attack the double bonds in the fatty acid

chains (Ayo et al, 2007). This rancidity could also result from the breakdown of unsaturated fatty acids in the oil in the presence of oxygen in the air to form peroxides.

The saponification value of the oil was 8.135mg/KOH indicating the oil contained mainly fatty acids of high molecular mass. This value compares favourably with saponification value of some standard oils which was based on the values and evidence that crude oils with low saponification numbers, have more long chain fatty acids and high molecular weight which is usually considered good for health purposes (Ayo et al, 2007). It was discovered that the oil's acid value was 15.147%, which generally indicated that it was edible. It was also found that the lower the acid value, the fewer free fatty acids it contained, making it less susceptible to rancidification, which is the process by which fats and oil hydrolyse when exposed to air, light, moisture, or bacteria, producing short-chain aldehydes, ketones, and free fatty acids. Also referred to as "rancidity," this term describes the chemical process by which fats and oils oxidise, giving food a disagreeable taste and odour as an outcome of the breakdown of lipids. It was discovered that the peroxide value was 38.6meq/kg. This oil's low peroxide value meant that it was less susceptible to oxidative rancidity at room temperature, which is the process by which fats and oils in food deteriorate into undesirable flavours, textures, and odours. This also applies to metals. The fact that the oil has a low iodine value is supported by the low peroxide value.

It was discovered that the oil had a density of 0.85g/mL. At 280°C, the oil fruit from the false wall had a viscosity of 1.5660 pa.s. Generally speaking, as intermolecular hydrogen bonding rises, so does oil's viscosity. This result indicates that the molecule has a few hydroxyl groups, but they haven't broken down yet. It was discovered that there were 7.574 percent free fatty acids in the oil. The oil's suitability for production and quality objectives was determined by the value of its free fatty acid. The lowest temperature at which the oil sample produced enough vapours under particular circumstances for the air-oil vapour mixture above the sample to ignite initially without reoccurring was known as the flash point.

37: Cooling Curve and Cooling Rate Determination of the False Wall (Canarium Schweinfurthii) Fruit Oil

The cooling time and rate measurements for 4140 steel probe tips in fake wall fruit oil were presented in the table below. The temperature was plotted from 850^0C to 200^0C at intervals of 50^0C+.The three cooling mechanisms that took place during the false wall fruit oil bath's quenching process the vapour blanket, boiling, and liquid cooling stages are represented by the cooling curve's shape. The cooling profile is, as anticipated, comparable to the majority of traditional oil cooling techniques. This is, of course, a violent performance. As the temperature of the oil bath rose during the liquid cooling stage, the rate of cooling of the false wall oil fruit slowed. This was influenced by the oil viscosity and the rate of convection.

According to experts like (Shuhui, 2007), agitation, quenchant viscosity, and bath temperature are some of the process variables that have an impact on heat transfer rates in this area. According to (Shuhui, 2007) research, the cooling rate rises as quenchant viscosity decreases, increasing the quenching oil's cooling capacity as the oil's temperature rises, peaks, and then falls again. Although in an austempering process, higher temperatures are involved in which viscosity has little or no effect during the quenching process. The viscosity was totally lost at these temperatures (450^0C - 250^0C). Figures 27 and 28 False Wall Fruit Oil at 40^0C Bath Temperature, The Cooling Curve of the Wall Fruit Oil at 40^0C Bath Temperature.

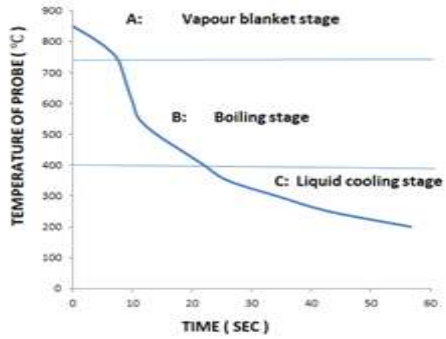

Figure 27: The Cooling Curve of the False Wall Fruit Oil at 40^{0}C Bath Temperature;

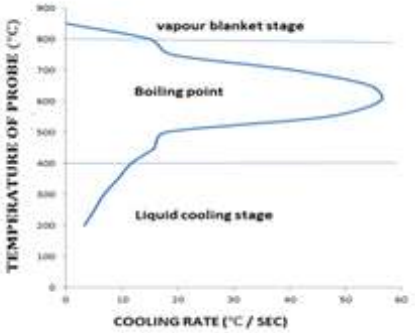

Figure 28 : The Cooling Rate of the False Wall Fruit Oil at 40^{0}C Bath Temperature

3.8 Comparisons of some Material Properties of Standard Gears with Trial Test Gears

3.8.1 Trial Test Gears:

Table 14 shows the mechanical property tests (tensile tests, elongation, and hardness values) obtained from the highest values generated from the molybdenum and vanadium alloyed addition elements during the austempering process of the ductile cast iron, which were used in the production of the gear samples. Plate 39 Austempered Molybdenum Alloyed ductile cast iron gear sample.Plate 40: Austempered Vanadium alloyed Ductile Cast Iron Gear Sample.Plate 41: Ductile Cast Iron from off the Shelf Domain

Table 14: ADI Trial Test Gears

oyed DI Austempered in se Wall (Canarium ıweinfurthii) Fruit Oil	**Tensile Strength (N/mm^2)**	**Elongation (%)**	**Hardness (BHN)**
lybdenum (Dm2)	741.8	10.3	581
ıadium (Dv2)	782.1	7.4	579

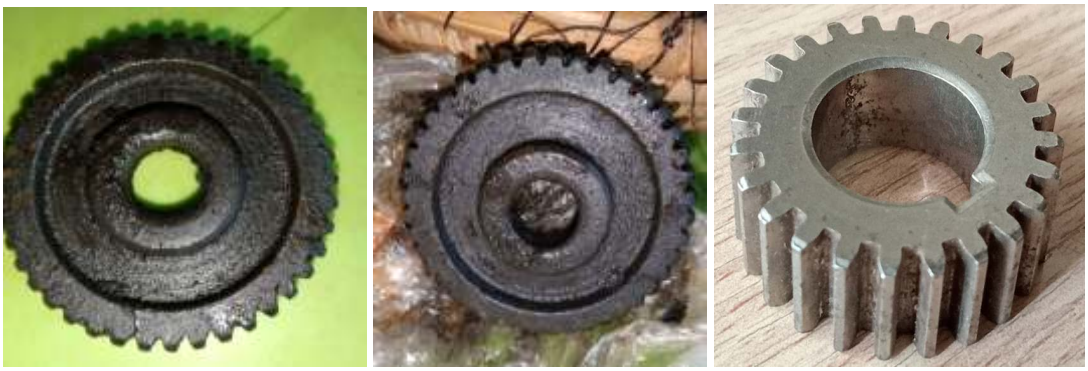

Plate 39Austempered Molybdenum Alloyed Ductile Cast Iron Gear Sample

Plate 40: Austempered Vanadium Alloyed Ductile Cast Iron Gear Sample

Plate 41: Ductile Cast Iron from off the Shelf Domain

3.9: Scanning Electron Microscope (SEM) Micrographs

Plates 42 - 45, show the Scanning Electron Microscope (SEM)microscope that were obtained from vanadium alloyed 3hrs optimum values generated for maximum ductility and at 4hrs for maximum strength for the oil alone and still the same thing that was seen at 3hrs and 4hrs with molybdenum under the same austempering medium.

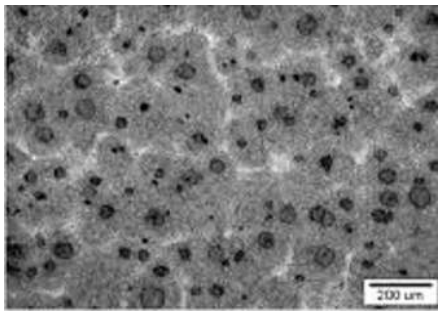

Plate 42: Alloyed (Dv2); 3hrs. Oil

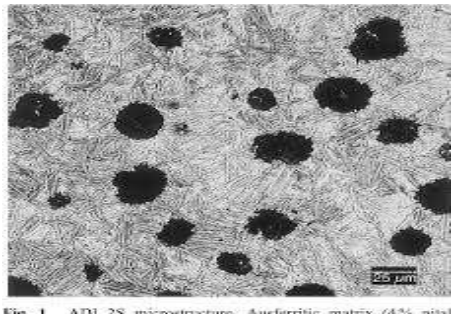

Plate 43: Alloyed Dv2; 4hrs Oil

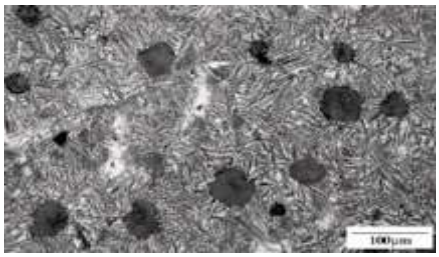

Plate 44: Alloyed (Dm3); 3hrs Oil

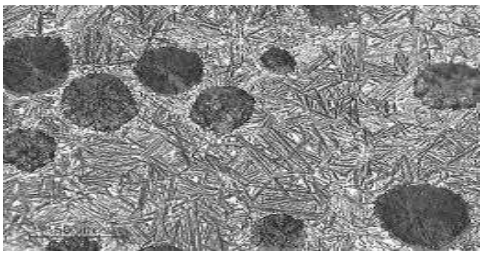

Plate 45: Alloyed (Dm3); 4hrs oil

4.0 CONCLUSION

According to the findings of the microstructural analysis and mechanical testing conducted for this study, the following conclusions have been reached.

1. The control specimen is A536 (65, 45, 12) grade ductile cast iron.
2. Each of the samples had a carbon equivalent (CE) of 4.2, which was adequate to cause graphitisation.
3. The unalloyed austempered specimens showed improved microstructural analysis and mechanical property tests as cannot be compared with the non-heat-treated unalloyed specimen.
4. The molybdenum alloyed austempered as-cast specimen showed molybdenum carbide (Mo_2C) which promoted the ferrite phase with increased nodule count, however, as the molybdenum weight percent increased, carbide formation increased.
5. The molybdenum alloyed austempered as-cast specimen showed an optimum property at 0.3wt%. The alloying element had little or no effect in altering the processing window (molybdenum does not delay the stage 1 reaction).
6. The vanadium alloyed austempered as-cast specimen showed an optimum property at 0.10wt% due to the formation of large volume of V_4C_3.
7. The processing window in this study showed that it occurred between 2hrs and 3hrs i.e optimum property tests were obtained at that time range in both austempering media.
8. The fruit oil can be a replacement or alternative for conventional salt bath during austempering heat treatment. However, the oil bath presented lower ductility and higher strength when compared to the salt bath.
9. The oil bath differed from the salt bath in the microstructure as the oil bath specimens showed more unreacted/undissolved carbides in their microstructures.
10. Mechanical properties of specimens alloyed with 0.1% vanadium at 3hrs showed, the optimum tensile strength was 784.6Mpa, 558BHN hardness, 58.65J impact energy, and 8.3% elongation for the salt bath and tensile strength of 782.1Mpa, 579BHN hardness, 62.76J impact energy and 7.4% elongation for the oil bath.

    At 4 hours austempering time, the specimens alloyed with 0.1wt % vanadium showed an optimum tensile strength of 996.7Mpa, 681BHN hardness, 69.94J impact energy, and 5.3%

elongation for the salt bath and tensile strength of 1025.3Mpa, 683BHN hardness, 72.78J impact energy and 4.3% elongation for the oil bath.
Mechanical properties of the specimens alloyed with 0.3% molybdenum at 3hrs showed, the optimum tensile strength was 773.34Mpa, 568BHN hardness, 49.6 impact energy, and 10.3% elongation for the salt bath and tensile strength of 806.5Mpa, 598BHN hardness, 52.28J impact energy and 11.05% elongation for the oil bath.
At 4 hrs austempering time, the specimens alloyed with the same 0.3% molybdenum showed an optimum tensile strength of 997.38Mpa, 697BHN hardness, 72.74J impact energy, and 6.7% elongation for the salt bath and tensile strength of 1099.6Mpa, 703BHN hardness, and 72.90J impact energy, and 5.4% elongation for the oil bath.

REFERENCES

Ingole, S., Rao, A., & Dutta Majumdar, J. (2012). Effect of alloying elements on graphitization of cast irons. Journal of Materials Engineering and Performance, 21(5), 721-728.

Kiani-Rashid, A. R., & Edmonds, D. V. (2009). Graphite nucleation and growth in cast irons. Journal of Materials Science, 44(10), 2604-2614.

Marcin, S., Piątkowski, J., & Staszczak, M. (2017). Influence of alloying elements on the microstructure and properties of nodular cast iron. Archives of Metallurgy and Materials, 62(2), 647-654.

Hernandez-Avila, J., Salinas-Rodriguez, E., Cerecedo-Saenz, E., Rivera-Landero, I., Cardoso-Legorreta, E., Flores-Badill, J., & Reyes-Valderrama, M. I. (2015). The Effect of Molybdenum on the Microstructure of Nodular Iron. European Scientific Journal, 11(36).

Farahat (2018): Farahat, A. I. Z. (2018). Hot Working of Ductile Iron Alloyed With Molybdenum. Journal of Materials Engineering and Performance, 27(10), 5321-5331.

Hernandez-Avila, J., Salinas-Rodriguez, E., Cerecedo-Saenz, E., Rivera-Landero, I., Cardoso-Legorreta, E., Flores-Badill, J., & Reyes-Valderrama, M. I. (2015). The Effect of Molybdenum on the Microstructure of Nodular Iron. European Scientific Journal, 11(36).

Rezvani, M., & Idris, J. (1997). The effect of vanadium on the microstructure and properties of cast irons. Journal of Materials Science, 32(16), 4399-4405.

Mao, Z., Farkoosh, A. R., & Seidman, D. N. (2025). Effects of Alloying Elements on Carbon Diffusion in the Austenite (F.C.C.)- and Ferrite (B.C.C.)-Phases. SSRN Electronic Journal. DOI: (link unavailable)

Putatunda, S. K. (2001). Influence of austempering temperature on microstructure and fracture toughness of a high-carbon, high-silicon, and high-manganese cast steel. Materials & Design, 22(8), 687-699.

T (2008): Evaluation of Hot Bitumen Bath as a Quenching medium for Austempering of Steel and Ductile Cast Iron, unpublished, PhD Thesis, Department of Metallurgical and Materials Engineering, Ahmadu Bello University Zaria.

, G., Sohala, S.R (2012): Effect of Copper on the properties of Austempered Ductile Iron castings. Bachelor thesis. Dept.of Metallurgical and Materials Engineering, National Institute of Technology Rourkela, India. Pp 19 - 21.

R, and Yadzani S. (1999): Influence of Molybdenum on Austempering behaviour of Ductile Cast Iron. Part 1 - Austempering kinetics of Ductile Cast Iron containing 0.13%Mo. Journal of Materials Science and Technology, 15: pp 233 - 240.

so, F (2010): Influence of Quench Rate on the Hardness obtained after Artificial Ageing of Al - Si - Mg Alloy. A thesis work performed at Jonkoping Institute of Technology Tekniska Hogskolan

S.B, Agboola J.B, Aigbodion V.S and Williams, E.J (2010): Hardening Characteristics of Plain Carbon Steel and Ductile Cast Iron using Neem Oil as Quenchant. Journal of Metallurgical and Materials Engineering, 5(1), pp 31 - 36.

S.B, Dauda E.T, Nyior G.B and Mohammed R.A (2007): Evaluation of local Vegetable oil as a Quenchants for Hardening Processin gray cast iron. Journal of Applied Science, Engineering and Technology, 7(2) pp 13 - 21.

al (2011): Evaluation of Khaya Senegalensis (Mahogany) Seed Oil as a Quenching Medium in Austempering Process of Ductile Cast Iron.

a, O.P (2002): Materials Science and Metallurgy: Dhan Pat Rai Publications Ltd pp 60 – 70.

s R.J, and Magalhaes I (2006): Micropitting of Austempered Ductile Iron Gears: Biogradeable Ester Vs. Mineral Revsta da Associacao Portuguesa de Analise, 13 (1) pp55 – 65.

p, K.S (2012): Effect of Austempering Temperature, time and copper addition on the Mechanical Properties of Austempered Ductile Iron. (Thesis, Department of Metallurgical and Materials Engineering, National Institute of Technology, Rourkela). Roll NO.28MM 102. (Unpublished)

A (2016): Potentials of Sesame Oil Bath as an Austempering Medium for Ductile Cast Iron.

sono W.J, Soemardi T.P, Suharno. B and Sulamet – Ariobimo R. D (2011). Effects of Carbon Equivalent on the Microstructures of Thin Wall Ductile Iron. Journal of Materials Science and Engineering 5, pp266 -270.

dani and R. Elliot (1999). Influence of molybdenum on austempering behaviour of ductile cast iron containing 0.45%Mo. Materials Science and Technology, August 1999 Vol. 15.

Lwin K (2009): Optimizing the Microstructure and Mechanical Properties of Austempered Ductile Iron, Journal of metals, Minerals and Materials. 18(2): pp 34 – 39.